Gasification of woody biomass under high heating rate conditions in pure CO2: Experiments and modelling

Chamseddine Guizani, Olivier Louisnard, Francisco Javier Escudero Sanz, Sylvain Salvador

Gasification of woody biomass under high heating rate conditions in pure CO_2: Experiments and modelling

C. Guizani*, O. Louisnard, F.J. Escudero Sanz, S. Salvador

RAPSODEE, Mines Albi, Route de Teillet, 81013, ALBI CT Cedex 09, France

Keywords:
Biomass
Pyrolysis
Gasification
CO_2
High heating rate
Numerical modelling

A B S T R A C T

The present paper focuses on the gasification of thin wood particles in pure CO_2 at 850 °C under high heating rate conditions (similar to fluidized bed gasifiers). The aim is to assess the potential use of CO_2 as gasifying medium and to learn more about its effects on the pyrolysis as well as on the char gasification stages. Experimental and numerical modelling results provide answers on the unfolding of the whole CO_2 biomass pyro gasification process. It was found that despite the CO_2 is present inside the particle during the pyrolysis stage, it has no noticeable impacts neither on the reaction rate nor on the char yield due to the relatively low temperature inside the particle. The CO_2 char gasification is the rate limiting step of the global pyro gasification reaction as its duration is near to 95% of the entire biomass con version time.

1. Introduction

Biomass to biofuels is considered to be one of the promising routes to cope with the fossil fuel depletion and to mitigate the green house gas emissions (mainly CO_2) causing numerous envi ronmental problems such as the global warming [1,2]. The CO_2 emissions are on the centre stage of the debate due to their continuously increasing amount in the atmosphere. Many research focus on possible ways to reduce them. Alternate fuels and value added products can be obtained from the conversion of carbon dioxide from simple molecules to higher hydrocarbon fuels and polymers following several techniques such as photo reduction, electrolysis, plasma, electro catalysis, dry reforming etc … [3].

Thermochemical conversion of biomass involves processes such as combustion, pyrolysis, liquefaction and gasification. The biomass pyro gasification encompasses two distinct stages: biomass pyrol ysis and char gasification. Biomass pyrolysis corresponds to the thermal decomposition of the fresh biomass into gas, tars and char. The pyrolysis product distribution depends on the biomass char acteristics (biomass type, chemical composition, particle size …) and process conditions (temperature, heating rate …) [4]. Char is a solid product of the biomass pyrolysis. It contains in major part carbon atoms with some hydrogen, oxygen, nitrogen and some minerals. The formed char reacts with the surrounding gasifying medium, O_2, H_2O, CO_2 or mixtures, yielding additional gases, namely CO_2, H_2 and CO, which amounts depend on the gasifying medium composition [5 7].

Biomass pyro gasification is conventionally operated with steam or air as gasifying medium but can also be performed using CO_2. Increasing number of studies dealing with coal and biomass thermochemical conversion are paying attention to CO_2 molecule as a gasifying agent [5,6,8]. For instance, it was demonstrated that introducing CO_2 with steam as a gasifying medium leads to an enhanced CO production [5,6,9]. Indeed, in the gas phases CO_2 can potentially react in the gas phase with hydrocarbons, such as methane, via a dry reforming reaction:

$$CO_2 + CH_4 \rightarrow 2H_2 + 2CO \quad \Delta H \quad +246.9 \text{ kJ/mol} \tag{1}$$

CO_2 can also react with hydrogen molecules according to the reverse water gas shift reaction (rWGS):

$$CO_2 + H_2 \rightarrow H_2O + CO \quad \Delta H \quad +41.2 \text{ kJ/mol} \tag{2}$$

Finally, in a biomass gasifier, CO_2 can react with the carbon of the char formed by the pyrolysis step, via the heterogeneous

* Corresponding author.
E-mail addresses: guizani.c@gmail.com (C. Guizani), louisnard@mines-albi.fr (O. Louisnard), javier.escuderosanz@mines-albi.fr (F.J.E. Sanz), sylvain.salvador@mines-albi.fr (S. Salvador).

Boudouard reaction:

$$C + CO_2 \rightarrow 2CO \quad \Delta H \qquad 179.5 \text{ kJ/mol} \tag{3}$$

Several authors also focused on the char gasification reaction under mixed atmospheres of H_2O and CO_2. Conclusions differ from a study to another on whether CO_2 inhibits the H_2O char gasification reaction, accelerates it or that the two reactants operate separately on the char surface [10 12]. In a previous study, we found experimentally that the CO_2 does not inhibit the H_2O char gasification reaction, but rather that the two gases cooperate and that the gasification rate in mixed atmospheres is the sum of the individual reactivities [13].

Renganathan et al. [14] performed a thermodynamic analysis of carbonaceous feedstocks gasification using CO_2 or mixtures of carbon dioxide with steam or oxygen and identified a universal optimal operating temperature of 850 °C for minimum energy input.

Other researchers [15] found that the use of CO_2 in biomass gasification in a fluidized bed gasifier increased substantially the carbon and energy conversion efficiency and decreased the amount of tars in the produced gas. The highest cold gas efficiency was achieved when gasifying biomass with CO_2.

The introduction of CO_2 as a reacting gas in biomass gasifier was also studied in Ref. [9] in the case of rice straw gasification. The authors studied the effect of the different gasification atmosphere compositions in H_2O, CO_2, O_2 and N_2 on the thermal efficiency of the gasification process, and came to the conclusion that the introduction of CO_2 has a positive effect on the thermal efficiency of a gasifier at temperature of 850 °C and above.

Other studies rather focused on the char gasification reaction with the aim of determining the kinetic parameters of the CO_2 char gasification reaction, or comparing the char gasification rates obtained with CO_2 and steam [16 18]. The effects of CO_2 on the pyrolysis process was also studied but less extensively than for the char gasification. CO_2 was found to influence the gas yield and composition as well as the char yield and properties [19 21]. In our previous work, we found that the major effects of CO_2 on the biomass pyrolysis are the increase of gas yield and modification of the char textural properties. However, the char reactivity to O_2, H_2O and CO_2 were practically the same as for char prepared under N_2 atmosphere [22].

Most of the modelling studies in the literature on biomass thermochemical conversion deal either with the sole pyrolysis step, or with the char gasification step only [17,18,23 27]. To the authors best knowledge, no previous studies deals with the entire gasification process of biomass in pure CO_2. In the present work, we focus on the whole woody biomass gasification process in the presence of pure CO_2 at a temperature of 850 °C. The objective of this paper is to learn more about the effect of CO_2 on the heterogeneous reactions of biomass pyrolysis and char gasification in high heating rates conditions typically encountered in fluidized bed gasifiers. The intent is also to not separate the pyrolysis from the char gasification step and to study the whole thermochemical conversion process as a single step reaction. In section 2, we will present the experimental device and procedure. Sections 3 and 4 will be dedicated to the numerical model and its implementation in COMSOL software. Experimental and modelling results will be presented in section 5.

2. Experimental study

2.1. Parent wood sample

Biomass samples are beech wood chips provided by SPPS Company (France). Raw samples were initially sieved. Biomass particle having a parallelepiped shape with a characteristic length L of 6 mm and a thickness Th of 1 mm were selected. Proximate and ultimate analysis of the biomass samples are presented in Table 1. The results are given on a dry basis. The moisture content of the wood chips was estimated to 10% ± 1%. The biomass particles were not further dried before the gasification experiments.

2.2. The macro thermogravimetry experimental device and procedure

The macro thermogravimetry M TG device is described in detail in our previous work on char gasification in mixed atmospheres of CO_2 and H_2O [13]. The platinum basket bearing the biomass particles is introduced in the hot reactor zone within 13 s. This procedure allows fast heating of the biomass particles and reproduces the conditions encountered in a fluidized bed gasifier. The pyrolysis experiments were performed at 850 °C, a typical temperature of a fluidized bed gasifier.

External heat transfer. The M TG reactor was characterized in terms of global heat transfer coefficient. The heat transfer coefficient was determined following a lumped heat capacitance method using a drilled steel sphere having a diameter of 5 mm and a Biot number inferior to 0.1. The heat transfer coefficient at 850 °C was found to be around 140 W/m^2 K [22] which is in the range of values for external heat transfer coefficients reported in the literature for fluidized bed gasifiers [23].

Reactor temperature profile. When introduced into the reactor, the biomass particles are not submitted directly to the hot zone temperature. The surrounding temperature increases along the z axis from the ambient to the final temperature. To establish the temperature profile along the z axis, we fixed a K type thermocouple to the platinum basket and introduced it in the reactor by steps of 7 cm and measured the temperature in each position up to final position of the basket inside the reactor. The results are shown in Fig. 1.

As the introduction speed is known (v = 7 cm/s), the temporal variation of the temperature surrounding the biomass particles reads:

$$\frac{dT_\infty}{dt} \quad \frac{dT_\infty}{dz}\frac{dz}{dt} \quad v\frac{dT_\infty}{dz} \tag{4}$$

dT_∞/dz is known from the temperature profile. The surrounding temperature is afterwards expressed as a polynomial function of the time $T_\infty(t)$ and is implemented in the model as an external condition related to reactor temperature.

Blank tests are performed prior to the pyrolysis experiment to account for the flowing gas dynamic pressure (force exerted on the basket) in addition to the drag forces along the ceramic tubes. Blank data are afterwards subtracted from the pyrolysis experiment ones. The blank tests as well as the experiments show a good repeatability [22]. The mean value of the relative standard deviations for the three tests (calculated as the mean of the relative standard deviations for all the experimental points from t = 0 s up to t = 600 s) is 5.9%.

Table 1
Proximate and ultimate analysis of the beech wood-chips (% dry basis).

Proximate analysis			Ultimate analysis			
VM	Ash	FC	C	H	O	N
88.1	0.4	11.5	46.1	5.5	47.9	0.1

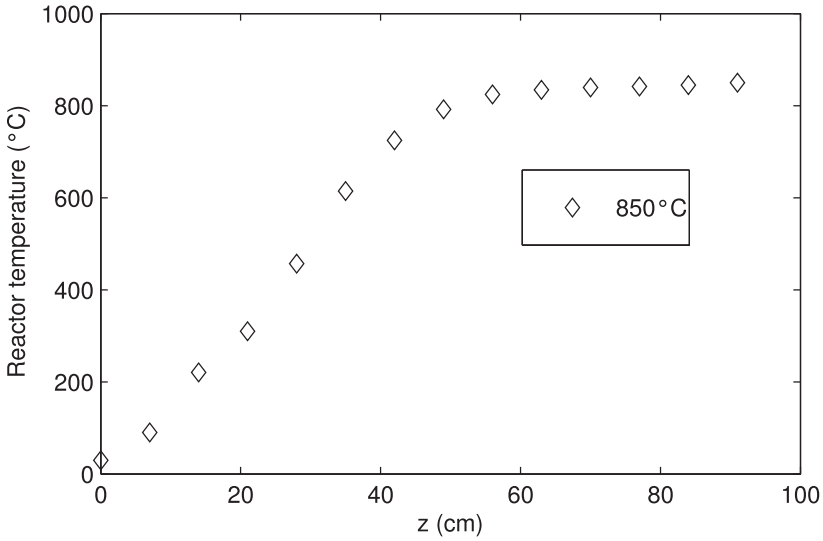

Fig. 1. Temperature profile in the M-TG reactor.

3. Numerical modelling of the CO_2 pyro-gasification

During the biomass CO_2 pyro gasification process, several phenomena are involved, including convective and radiative heat transfer between the biomass particle, the surrounding gas and the reactor walls, conductive and internal radiative heat transfer respectively through the particle solid phase and in the pores, chemical reactions, chemical species transport, shrinking etc … To model the physics underlying the process, we established mass and energy balance equations and considered several assumptions to render the model tractable:

- A 2D geometry is used due to similarity between the tangential and radial properties in the wood/char
- Local thermodynamic equilibrium between the solid and the gas phase
- No particle shrinking is taken into account
- Char is assimilated to pure carbon
- Darcy's law is used to determine the gas velocity in the solid matrix
- In Darcy's law, we use an isotropic permeability, since the large difference of permeabilities between the radial and the fibre direction induces numerical convergence problems.
- All gaseous species are assumed to follow a Fick diffusion law, with the same isotropic diffusion coefficient.
- Chemical reactions follow Arrhenius law and are first order reactions with respect to the reactants.

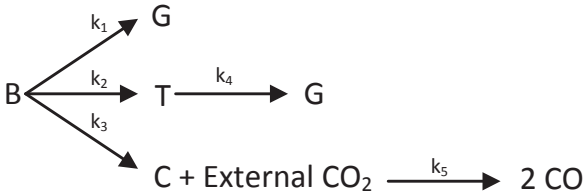

Fig. 2. CO_2 pyro-gasification reaction scheme.

3.1. Kinetic scheme

The CO_2 pyro gasification reactions scheme is shown in Fig. 2. The indices B, G, T and C in the scheme as well as in the equations refer respectively to the fresh biomass, gas, tars and char. It gathers the pyrolysis and the char gasification steps. The pyrolysis stage includes three parallel reactions where the initial wood decomposes into gas (R1), tars (R2) and char (R3), with defined mass stoichiometric coefficients. Tars are afterwards cracked into gas following the secondary reaction (R4). The mass stoichiometric coefficients are noted ω_C, ω_G and ω_T for char, gas and tars respectively.

$$\omega_C + \omega_G + \omega_T \quad 1 \tag{5}$$

The char yield was fixed at 0.12 (according to our experimental data). The tar yield was fixed to 0.05 and the gas yield is given by the difference to the unity. The char gasification corresponds to the reaction (R5) where the surrounding CO_2 reacts with the char following the Boudouard reaction to form CO.

3.2. Mass conservation equations

3.2.1. Solid species

Biomass and char are solid species. The conservation equations for these latter do not include transport terms.

Biomass decomposition is described by the following equation:

$$\frac{\partial \rho_B}{\partial t} \quad (\omega_G k_1 + \omega_T k_2 + \omega_C k_3)\rho_B \tag{6}$$

Char formation and gasification is given by:

$$\frac{\partial \rho_C}{\partial t} \quad \omega_C k_3 \rho_B \quad k_5 \rho_C P_{CO_2} \tag{7}$$

The first term on the right hand side accounts for char formation, while the second accounts for the char gasification reaction. ρ refers to the density kg m^{-3} while k_i refers to the reaction rate s^{-1} constant given by an Arrhenius law.

3.2.2. Gaseous species

Four gaseous species are considered:

- CO_2, which is the surrounding gas in the reactor. The particles void is considered to be initially filled with CO_2.
- Gas, representing the pyrolysis gas emitted by the wood decomposition reaction. An average molecular weight of 22 g/mol was calculated for the pyrolysis gas based on the work of Couhert et al. [28].
- Tars, the heavy condensible gases assumed to have a molecular weight of 78 g/mol.
- CO, which is the product of the CO_2 char gasification reaction (R5).

The CO_2 conservation equation reads:

$$\frac{\partial \varepsilon \rho_{CO_2}}{\partial t} + \nabla \cdot \left(\rho_{CO_2} \mathbf{v} \quad D_{eff} \nabla \rho_{CO_2} \right) \qquad k_5 \rho_C P_{CO_2} \tag{8}$$

The pyrolysis gas conservation equation reads:

$$\frac{\partial \varepsilon \rho_G}{\partial t} + \nabla \cdot \left(\rho_G \mathbf{v} \quad D_{eff} \nabla \rho_G \right) \qquad \omega_G k_1 \rho_B + \omega_T \varepsilon k_4 \rho_T \tag{9}$$

The tars conservation equation reads:

$$\frac{\partial \varepsilon \rho_T}{\partial t} + \nabla \cdot \left(\rho_T \mathbf{v} \quad D_{eff} \nabla \rho_T \right) \qquad \omega_T (k_2 \rho_B \quad \varepsilon k_4 \rho_T) \tag{10}$$

The CO conservation equation reads:

$$\frac{\partial \varepsilon \rho_{CO}}{\partial t} + \nabla \cdot \left(\rho_{CO} \mathbf{v} \quad D_{eff} \nabla \rho_{CO} \right) \qquad + k_5 \rho_C P_{CO_2}^n \tag{11}$$

ε, $\mathbf{v}$ and D_{eff} are respectively the solid particle porosity, the gas velocity m s^{-1} vector and the effective diffusion coefficient m^2 s^{-1}.

3.3. Momentum conservation

The gas phase momentum equation in the porous media is expressed through a Darcy's Law. The superficial velocity is expressed as:

$$\mathbf{v} \qquad \frac{K}{\mu} \nabla P, \tag{12}$$

where K and μ are respectively the average permeability and the gas viscosity. As the permeability in the grain direction is far greater than in the radial direction we considered an average permeability for the two directions to ensure the numerical convergence. The total pressure is expressed by using the ideal gas law and summing the pressure contribution of all the gas species:

$$P \qquad \left(\frac{\rho_G}{M_G} + \frac{\rho_{CO_2}}{M_{CO_2}} + \frac{\rho_T}{M_T} + \frac{\rho_{CO}}{M_{CO}} \right) RT \tag{13}$$

R refers to the universal gas constant J mol^{-1} K^{-1} and M_i refers to the molecular weight kg mol^{-1}.

3.4. Energy conservation equation

The energy conservation equations is formulated with the assumptions of constant particle volume and a local thermal equilibrium between solids and gases:

$$\frac{\partial \mathscr{H}}{\partial t} + \nabla \cdot \sum_i h_i \mathbf{N}_i \qquad \nabla \cdot \mathbf{q} \tag{14}$$

The first term on the left hand side of the equation represents the time derivative of the total enthalpy per unit volume J s^{-1} m^{-3} with:

$$\mathscr{H} \qquad \sum_{i \quad B,C,G,T,CO_2,CO} \rho_i h_i$$

with h_i representing the specific enthalpy of "i" J kg^{-1}. The total enthalpy time derivative can be expressed in a more extended form as:

$$\left(\rho_B C_{pB} + \rho_C C_{pC} + \varepsilon \rho_G C_{pG} + \varepsilon \rho_T C_{pT} + \varepsilon \rho_{CO_2} C_{pCO_2} \right) \frac{\partial T}{\partial t} + \nabla \cdot \sum_i h_i \mathbf{N}_i$$

$$\nabla \cdot \mathbf{q} + Q \tag{15}$$

$\mathbf{N}_i$ refers to the mass flux of "i" kg m^{-2} s^{-1}.

The second term on the left hand side of the equation represents the convective and diffusive transport of energy, with:

$$\sum_{i \quad G,T,CO_2,CO} h_i \mathbf{N}_i \qquad \mathbf{v} \left(\sum_{i \quad G,T,CO_2,CO} \rho_i h_i \right) \qquad D_{eff} \left(\sum_{i \quad G,T,CO_2,CO} h_i \nabla \rho_i \right)$$

$\mathbf{q}$ is the conductive heat flux W m^{-2} inside the porous media expressed by Fourier's law:

$$\mathbf{q} \qquad \bar{\bar{\lambda}} \nabla T$$

where $\bar{\bar{\lambda}}$ is the effective thermal conductivity tensor W m^{-1} K^{-1} taking into account the radiative heat transfer inside the pores.

$\dot{Q}$ accounts for the energy released/consumed by the different reactions R(1) R(5), as well as for the differences of sensible heats between the products and reactants of these reactions W m^{-3}. This formulation of the source term was introduced by Haseli et al. [25].

$$\begin{aligned} Q \qquad & \left(\omega_G \rho_B k_1 \left(\Delta H_{B-G} + \int (C_{pB} \quad C_{pG}) dT \right) \right. \\ & + \omega_T \rho_B k_2 \left(\Delta H_{B-T} + \int (C_{pT} \quad C_{pB}) dT \right) \\ & + \omega_C \rho_B k_3 \left(\Delta H_{B-C} + \int (C_{pC} \quad C_{pB}) dT \right) \\ & + \omega_T \varepsilon \rho_T k_4 \left(\Delta H_{T-G} + \int (C_{pG} \quad C_{pT}) dT \right) \\ & \left. + k_5 \rho_C P_{CO_2} \left(\Delta H_{Boudouard} + \int (C_{pCO_2} \quad C_{pCO}) dT \right) \right) \end{aligned}$$

3.5. Initial and boundary conditions

3.5.1. Initial conditions

Seven initial conditions are identified for the model variables including the density of the different species and the temperature. The temperature is initially uniform in the particle and fixed to 293 K. The particle porosity is assumed to be filled with CO_2 at the atmospheric pressure.

$$\rho_B(\mathbf{r}, t \quad 0) \quad \rho_B^0 \tag{16}$$

$$\rho_C(\mathbf{r}, t \quad 0) \quad 0 \tag{17}$$

$$\rho_G(\mathbf{r}, t \quad 0) \quad 0 \tag{18}$$

$$\rho_T(\mathbf{r}, t \quad 0) \quad \rho_T^0(\mathbf{r}) \tag{19}$$

$$\rho_{CO}(\mathbf{r}, t \quad 0) \quad 0 \tag{20}$$

$$\rho_{CO_2}(\mathbf{r}, t \quad 0) \quad M_{CO_2}\left(\frac{P^0(\mathbf{r})}{RT^0}\right) \tag{21}$$

$$T(\mathbf{r}, t \quad 0) \quad 293K \tag{22}$$

3.5.2. Boundary conditions

At the particle surface. For gas, tars and CO, a flux condition is considered at the particle surface: the gas flux at the particle surface is proportional to the difference between the concentration $\rho_i^{\partial\Omega}$ at the particle surface and that in the surrounding ρ_i^{∞}.

$$\mathbf{N}_i^{\partial\Omega} \cdot \mathbf{n} \quad k_m\left(\rho_i^{\partial\Omega} \quad \rho_i^{\infty}\right) \quad i \quad G, T, CO \tag{23}$$

where k_m is the convective mass transfer coefficient m s^{-1}, and the total gas flux $N_i^{\partial\Omega}$ is the sum of convective and diffusive terms:

$$\mathbf{N}_i^{\partial\Omega} \quad \left(\rho_i \mathbf{v} \quad D_{eff} \nabla \rho_i\right)^{\partial\Omega} \tag{24}$$

Since the surrounding gas is assumed to be pure CO_2, we set $\rho_i^{\infty} = 0$, i = G, T, CO.

For the surrounding gas (CO_2), the boundary condition is obtained by fixing the total pressure at the particle surface as $P^{\partial\Omega} = P^{\infty}$. Using equation (13) gives the concentration of the CO_2 specie at the particle surface:

$$\rho_{CO_2}^{\partial\Omega} \quad M_{CO_2}\left(\frac{P^{\infty}}{RT^{\partial\Omega}} \quad \frac{\rho_G^{\partial\Omega}}{M_G} \quad \frac{\rho_T^{\partial\Omega}}{M_T} \quad \frac{\rho_{CO}^{\partial\Omega}}{M_{CO}}\right) \tag{25}$$

The heat flux continuity at the particle surface leads to the following boundary condition:

$$\mathbf{q}^{\partial\Omega} \cdot \mathbf{n} \quad h_{conv}(T_{\infty} \quad T) + \sigma\xi\left(T_{\infty}^4 \quad T^4\right) \tag{26}$$

where h_{conv} (W m^{-2} K^{-1}) is the convective heat transfer coefficient.

k_m as well as h_{conv} are determined by using correlations based on Nusselt and Sherwood numbers for a flow over a thin slab:

$$Nu \quad 0.644\, Re^{0.5}\, Pr^{0.343} \tag{27}$$

$$Sh \quad 0.644\, Re^{0.5}\, Sc^{0.343} \tag{28}$$

where Re, Pr and Sc are respectively the Reynolds, Prandlt and Schmidt numbers, functions of the surrounding gas (CO_2) properties and flow characteristics. Finally, σ is the Stephan Boltzmann coefficient W m^{-2} K^{-4} and ξ is the particle emissivity.

At the particle mid planes. A symmetry condition is considered at the particle mid planes ($x, y = Th/2$) and ($x = L/2, y$):

$$\mathbf{N}_i^{mid} \cdot \mathbf{n} \quad 0 \tag{29}$$

$$\mathbf{q}^{mid} \cdot \mathbf{n} \quad 0 \tag{30}$$

3.6. Kinetic parameters, heat of reactions and thermo physical properties

Kinetic parameters, heat of reactions and thermo physical properties (porosity, permeability, thermal conductivity, pore diameter, emissivity) were identified from the literature based on biomass pyro gasification studies. The data are summarized in Tables 2 4. The physical properties of the solid blend biomass + char during the pyrolysis are calculated as linear combinations of the properties of char and biomass following:

$$\text{Prop} \quad \text{Prop}_B \frac{\rho_B}{\rho_{B0}} + \text{Prop}_C\left(1 \quad \frac{\rho_B}{\rho_{B0}}\right) \tag{31}$$

3.7. The geometry

A two dimensional model is considered for the CO_2 pyro gasification model. The biomass particle is assimilated to a rectangle which corners are reshaped for a better numerical convergence. The biomass particle has a thickness Th = 1 mm and a length L = 6 mm. Because of the symmetry at the particle centre, only a quarter of the biomass particle can be considered. The particle geometry and meshing is shown in Fig. 3. The mesh size is reduced near the surface for a better numerical convergence. The model sensitivity to the mesh size was tested by reducing the mesh size by a half.

4. COMSOL modelling

CO_2 pyro gasification experiments were modelled using 3 modules in COMSOL software: "*Mathematics*", "*Transport of diluted species*" and "*Heat transfer in fluids*". The first one is used to define the ordinary differential equations (ODEs) related to the conservation of solid species (wood + char). The second and third modules are used to describe mass and heat transfer inside the porous media. The former is used for the mass conservation of the gaseous species and the latter is used to set the energy conservation equation. COMSOL software has pre defined forms for the conservation equations which are not consistent with the above described set equations. Some mathematical transformations of the latter are therefore needed so that it fits into the COMSOL formalism. Details about the mathematical transformation of the conservation equations are presented in appendix A.

5. Results and discussion

5.1. CO_2 pyro gasification experimental results

Fig. 4, which represents the normalized mass loss vs. time, shows three repeatability tests of the CO_2 pyro gasification. The experiments are very reproducible and the plots are almost superposed. The biomass pyro gasification in CO_2 shows two major steps, namely the wood pyrolysis and the char gasification. The pyrolysis stage lasts 30 times less than the char gasification one. The former takes 20 s (including the heating stage) while the latter lasts for near to 600 s. Clearly, the char gasification is the rate limiting step in the total pyro gasification process.

In order to assess the effect of using pure CO_2 on the pyrolysis step, it is suitable to compare the CO_2 pyrolysis with a reference one in a N_2 atmosphere. The results are shown in Fig. 5. The time scale was reduced to 200 s to highlight the pyrolysis stage and the beginning of the char gasification. During the pyrolysis active phase the rate of mass loss is almost the same in the N_2 and CO_2 pyrolysis atmospheres. No influence of the CO_2 can be perceived during this stage. We observed also that the char yield is almost the same. We expected that less char would be formed during the pyrolysis in pure CO_2 since we had found previously that in a that in a mixture of 20% CO_2 in N_2 pyrolysis atmosphere, the char yield decreased by

Table 2
Thermophysical properties.

Thermophysical property	Value/correlation	References
Thermal conductivity (W/m·K)	$\lambda_{B\ grain}$ 0.25 $\lambda_{B\ radial}$ 0.1 $\lambda_{C\ grain}$ 0.1 $\lambda_{C\ radial}$ 0.07	[25]
Permeability (cm^2)	$K_{B\ grain}$ $5\cdot10^{-12}$ $K_{B\ radial}$ $5\cdot10^{-12}$ $K_{C\ grain}$ 10^{-9} $K_{C\ radial}$ 10^{-9}	[25]
Viscosity (Pa·s)	μ $4.35\cdot10^{-5}$ for all the gas species	[34]
Pore diameter (cm)	dp_B $5\cdot10^{-3}$ dp_C 10^{-2}	[25]
Porosity	ε_B 0.3 ε_C $1-(1-\varepsilon_B)\omega_C$	[25]
Tortuosity	τ 3	[35]
Heat capacity (J/kg·K)	C_{pB} $1.5+10^{-3}T$ C_{pC} $0.44+2\,10^{-3}T-6.7\,10^{-7}T^2$ C_{pG} $0.761+7\,10^{-4}T-2\,10^{-7}T^2$ C_{pT} $-0.162+4.6\,10^{-3}T-2\,10^{-6}T^2$ C_{pCO_2} $24.997+55.186\theta-33.691\theta^2+7.948\theta^3-0.1366/\theta^2$ C_{pCO} $25.567+6.0961\theta+4.0546\theta^2-2.6713\theta^3+0.1310/\theta^2$ θ $1000/T(K)$	[25]
Emissivity	ξ_B 0.6 ξ_C 1	[24]
Molecular diffusivity (m^2/s)	D_{eff} $\frac{\varepsilon}{\tau}\frac{1}{\left(\frac{1}{D_{Knudsen}}+\frac{1}{D}\right)}$ D $\left(\left(1.67\cdot10^{-5}\frac{T}{298}\right)^{1.75}\right)$ for all the gas species $D_{Knudsen}$ $0.97(d_p/2)(T/M_i)^{0.5}$	[34]

Table 3
Kinetic parameters.

Reaction rate constant (s^{-1})	Pre-exponential factor, A (s^{-1})	Activation energy (kJ/mol)	References
k_1	$1.3\cdot10^8$	140	[36]
k_2	$2\cdot10^8$	133	[36]
k_3	$1.08\cdot10^7$	121	[36]
k_4	$3.2\cdot10^4$	72.8	[25]
k_5	$1.04\cdot10^2$	200	Adjusted

Table 4
Heat of reactions.

Reaction	Heat of reaction (kJ/kg)	References
1	418	[36]
2	418	[36]
3	418	[36]
4	−42	[36]
4	179.5	[6]

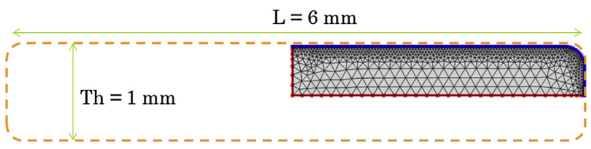

Fig. 3. Geometry and meshing of a quarter of the biomass particle.

near to 1% and imputed it to the gasification of the nascent char among the plausible explanations [22]. Other researchers have found that the coal char yield decreases in a pure CO_2 atmosphere compared to the pyrolysis in a He atmosphere [8], and was also attributed to the gasification of the nascent char. For biomass chars, the routes may be different for high CO_2 concentrations. Indeed, Watanabe et al. [21] found that in the case of lignin pyrolysis, the pure CO_2 atmosphere induces the formation of more char than in an argon atmosphere. The CO_2 was found to react with metal salts present in the lignin structures (K, Na) and forms carbonates (Na_2CO_3 or K_2CO_3). For metal depleted lignin, the char yield in an Ar or a CO_2 atmosphere were the same. The gasification of nascent char, and the formation of carbonates on the char surface have opposite effects which may lead, in our case, to a similar char yield as in an N_2 atmosphere.

The major mass loss occurs between t = 10 s and t = 16 s. In this time interval, the particle loses near to 80% of its mass. Follows a slower mass decay until 25 s after which the char mass was constant. The pyrolysis stage can be divided into two phases: the active phase where the major mass loss occurs, and the passive phase where the mass loss rate is far smaller than in the active phase. Under the N_2 and CO_2 atmospheres, the char mass reached respectively an almost constant value at t = 25 s: 0.116 and 0.123. In a CO_2 atmosphere, there is an almost constant plateau followed by the char gasification stage which started at 35 s while the char mass remained constant in the N_2 atmosphere. The char gasification and pyrolysis steps seems to be independent and not overlapping. The presence of the 10 s plateau before the starting of the gasification will be discussed in the next sections.

5.2. Modelling results

Fig. 6 shows the modelling results in terms of normalized mass versus time compared to the experimental data. As visible on the

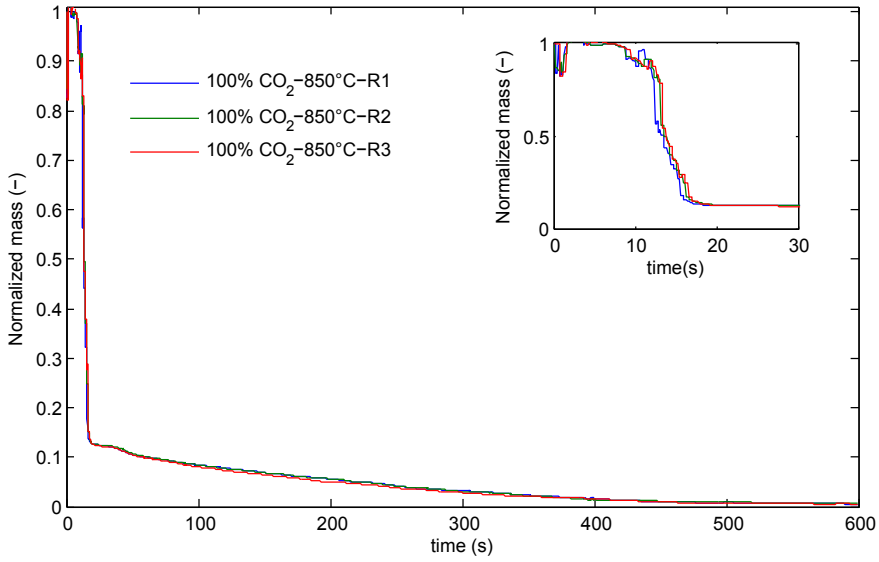

Fig. 4. Pyro-gasification in pure CO_2: normalized mass VS time.

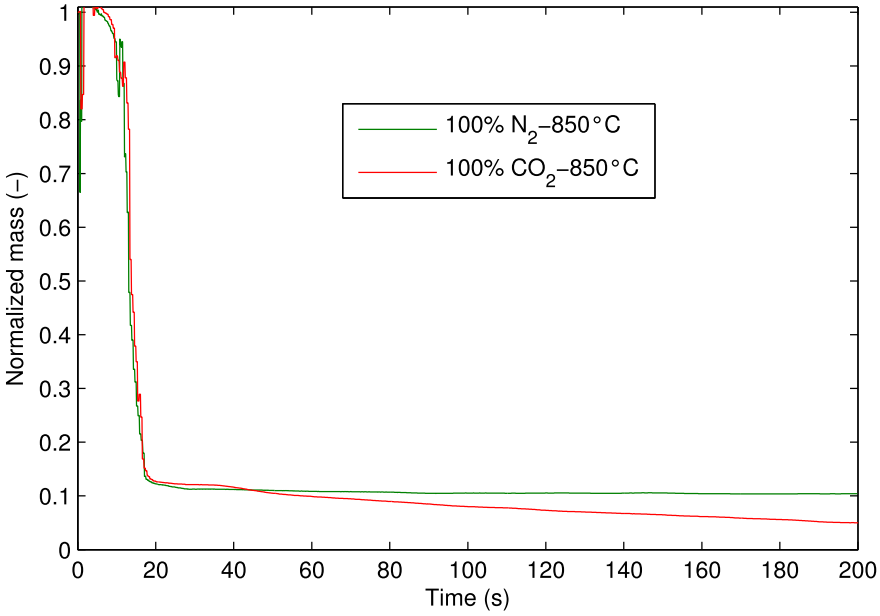

Fig. 5. Pyro-gasification in pure CO_2 VS N_2 pyrolysis.

figure, the model predicts very well the experimental data. Some small discrepancies are nonetheless observable. In order to high light the agreement of the numerical model with the experimental data, we made a focus on the pyrolysis stage in Fig. 7 a, on the transition stage in Fig. 7 b and another one on the char gasification stage in Fig. 7 c. In the very beginning of the normalized mass vs. time curve (at around 2 3 s), we can note an abrupt mass decrease followed by an increase. This artefact has nothing to do with the pyrolysis reaction, but is related to the mechanical forces when moving the weighing system upward. Only the very beginning of the weighing device introduction process is poorly reproducible. The numerical model describes correctly the heating stage as well as the pyrolysis stage. There are small discrepancies between the model and the experimental data in the beginning and in the end of the pyrolysis, still, they are acceptable. The model captures well the transition (25 35 s plateau) between the end of the pyrolysis (at 25 s) and the beginning of the char gasification (at 35 s). The char gasification is correctly described by the model with a good accu racy. The activation energy for the CO_2 char gasification reaction was adjusted to 200 kJ/mol and is in the range of values presented in Di Blasi's review on combustion and gasification rates of ligno cellulosic chars [7].

5.2.1. Pyrolysis stage analysis

When introduced into the hot reactor, the wood particles are heated by radiation with the hot gas and the reactor wall and by convection with the surrounding hot gas. As the wood particles are not thermally thin bodies (Biot number $\simeq 0.1$), there exists a

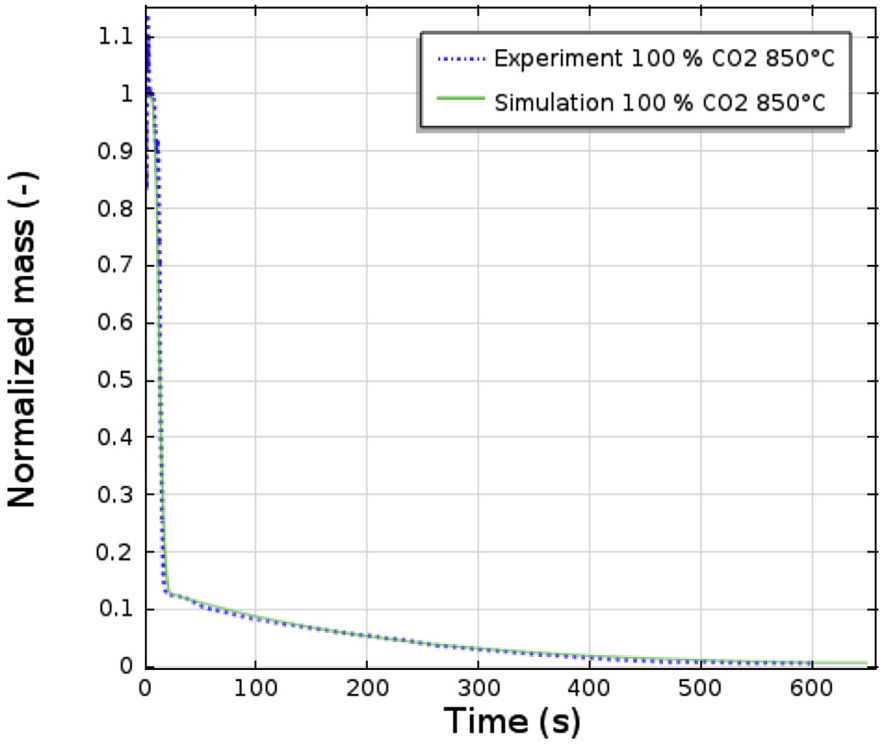

Fig. 6. CO_2 pyro-gasification modelling results.

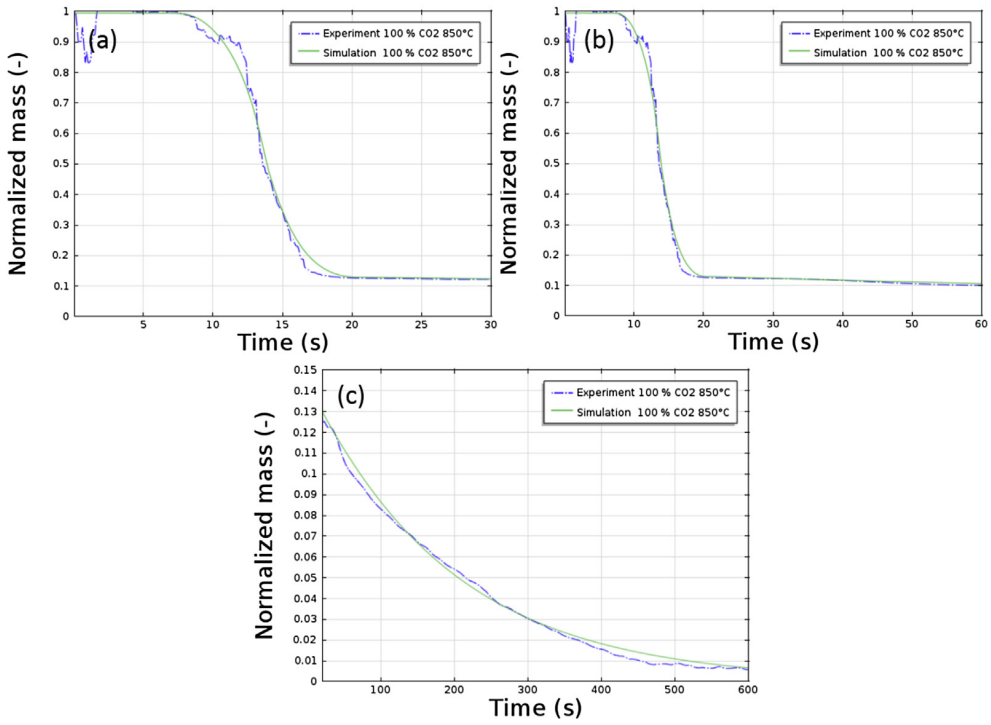

Fig. 7. A zoom on the pyrolysis stage (a), on the transition between the pyrolysis and char gasification stages (b) and on the char gasification stage (c).

temperature gradient between the surface and the particle centre. This temperature difference would become smaller and smaller as the particle becomes thinner. To illustrate this spatial temperature difference, the time variations of the temperatures on the particle surface and in the centre is shown in Fig. 8. A semi log scale is adopted to enhance readability. It can be seen that the temperature

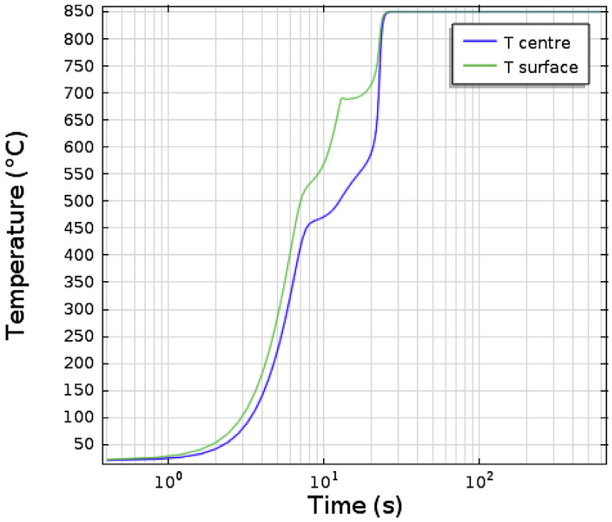

Fig. 8. Temperature evolution at the particle surface and centre during the pyro-gasification process.

increases differently at the particle surface and centre. During the heating stage, the energy received from the surroundings heats the particle surface, and heat is transported by conduction towards the centre. As the biomass pyrolysis reaction starts, part of the energy received is consumed by the endothermic pyrolysis reaction as chemical bonds are disrupted. A temperature near plateau is observed around 11 s. The temperature plateau observed corre sponds to a steady state phase where the energy extracted from the hot surroundings exactly balances the energy sucked by the reac tion in the whole particle. This temperature evolution behaviour was noticed in previous studies [29 31]. This has to be taken with caution, since no experimental measure of the surface temperature was performed. Contour plots of the fresh biomass mass fraction are shown in Fig. 9 at different reaction times. The black regions correspond to pure char, whereas the white ones correspond to fresh wood. The region where the fresh biomass mass fraction is equal to zero (black coloured) denotes that the solid corresponds only to char. While the outer regions of the particle are pyrolysed with production gas and char, the inner regions can contain fresh wood. At 18 s almost all the initial fresh biomass is pyrolysed.

When the biomass decomposes, the solid porosity increases and the released gaseous compound fill the porous void. The porosity evolution at the particle surface as well as in the centre predicted by the model is shown in Fig. 10. The same time delay as for the temperature increase is noticed for the porosity evolution. As the chemical reaction rate is not uniform throughout the particle due to the non uniformity of the temperature, less wood is dissociated near the centre than near the surface. This impacts the porosity which increases more rapidly at the surface. It can be also noticed that the difference between the porosity evolution at these two respective locations vanishes as soon as the gasification of the char begins. This attests of the homogeneity of the char gasification reaction throughout the char particle.

During the wood pyrolysis, the presence of gaseous species in side the pores induces a pressure increase. As for temperature, the total pressure evolution at the particle surface and centre is plotted in Fig. 11. The pressure at the surface remains constant as it is a fixed boundary condition. At the particle centre, the pressure initially decreases. The temperature gradient between the particle surface and centre induces a CO_2 concentration gradient, leading to a CO_2 flow toward the surface. Afterwards, the pressure increases as the pyrolysis begins with the production of gaseous species. Two pressure peaks can be noticed. This phenomena is due to the competition between the two mechanisms of Darcy and Fick diffusion which govern the gas species transport inside the particle. Simulation results show that the pressure reaches a maximum of 132 kPa at the centre of the particle. Similar values are reported in the literature [25,32]. During the gasification stage the pressure remains constant throughout the particle. This will be discussed latter on.

Colour map plots of the gas + tar mass fraction $\frac{(\rho_C+\rho_T)}{(\rho_C+\rho_T+\rho_{CO}+\rho_{CO_2})}$ in the pore space are shown in Fig. 12 at 12 s, 14 s, 16 s, 18 s and 20 s. The difference to the unity represents the $CO_2 + CO$ mass fraction in the pore space. Initially, part of the CO_2 leaves the particle during the heating stage as discussed before. During the heating stage, the temperature gradient inside the particle causes a concentration gradient leading to a CO_2 flux toward the surface according to Fick's law. Part of the CO_2 remains in the particle porosity during the heating stage. When chemical reactions start with production of

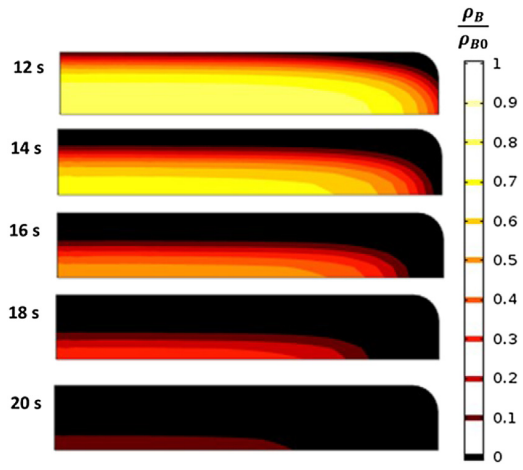

Fig. 9. Contour plots of the fresh wood mass fraction along the conversion at 12 s, 14 s, 16 s, 18 s and 20 s.

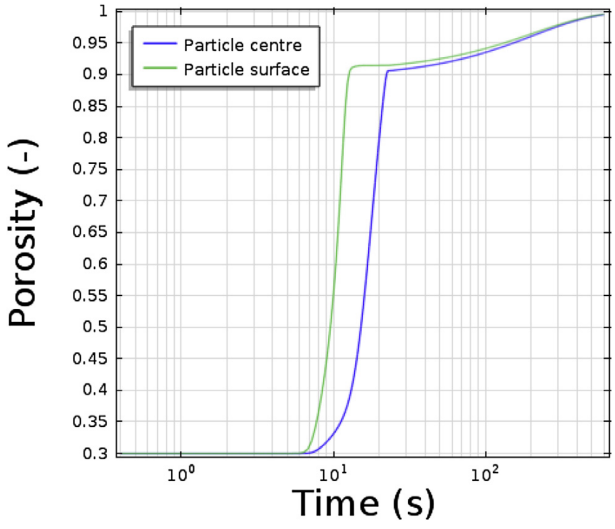

Fig. 10. Porosity evolution at the particle surface and centre during the pyro-gasification process.

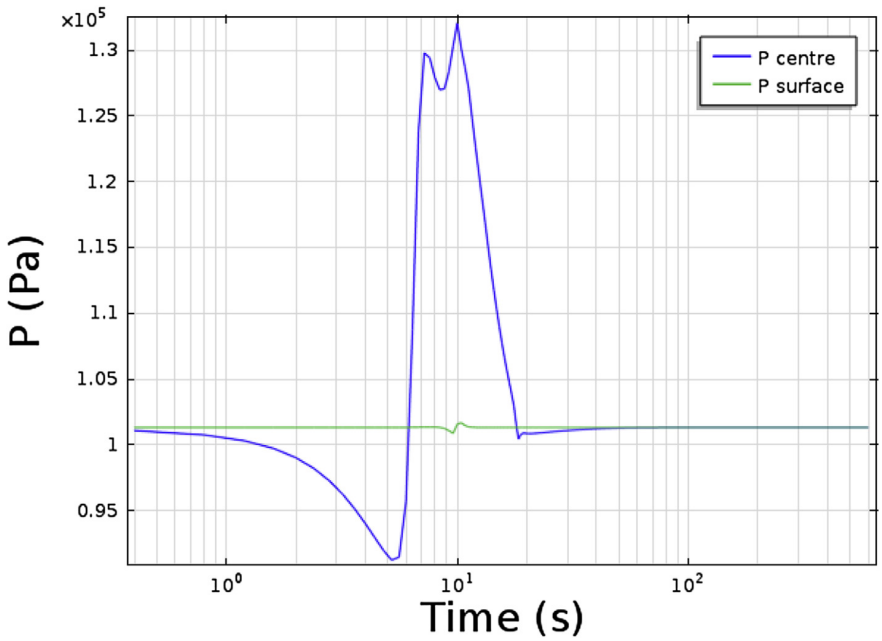

Fig. 11. Pressure evolution at the particle surface and centre during the pyro-gasification process.

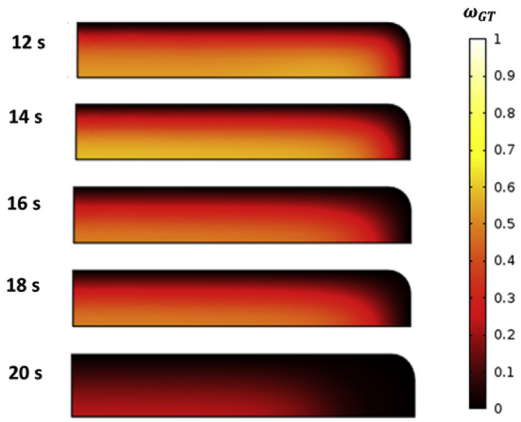

Fig. 12. Colour map plots of the gas + tar mass fraction in the gaseous phase at 12 s, 14 s, 16 s, 18 s and 20 s. (For interpretation of the references to colour in this figure legend, the reader is referred to the web version of this article.)

gas and tars, the CO_2 remaining in the particle becomes mixed with these latter inside the particle porosity. Due to the concentration difference and pressure gradients, gas and tars leave the particle. Simultaneously, the CO_2 concentration difference between the particle surface and the internal regions induces an inward CO_2 diffusive flux. The CO_2 concentration increases with time inside the particle.

What is the impact of CO_2 during the pyrolysis stage? According to the previous observations and discussion about the presence of CO_2 inside the particle during the pyrolysis stage, even if non uniformly distributed, one can expect that it begins to react with the char as soon as formed. Nevertheless, the Boudouard reaction has a very low rate at low temperature, so that even if CO_2 is present in certain regions, without a sufficiently high temperature the reaction term accounting for CO_2 consumption would be negligible. To highlight this assertion, colour map plots of CO_2 partial pressure as well as contour plots of the temperature are plotted in Fig. 13. Despite the CO_2 is present in the particle, even with a considerable partial pressure, the char gasification reaction can not take place as the temperature is not high enough. For instance, at t = 18 s, one can notice that in a part of the particle, the CO_2 partial pressure reaches 50 kPa at a temperature of 650 °C while in another outer region, it reaches 90 kPa at a temperature of 790 °C. The gasification reaction rate is not sufficiently high to induce a noticeable mass loss in these conditions.

5.2.2. Analysis of the char gasification stage

The char gasification stage is the rate limiting step in the pyro gasification process. The temperature, and the pressure as shown in Figs. 8 and 11 are uniform throughout the particle and constant along the conversion. Once the pyrolysis stage is finished, all the remaining char porosity is filled with CO_2. This latter reacts with the char to produce CO via the Boudouard reaction. The char void remains all mostly filled with CO_2 along the char conversion. The CO_2 mass fraction in the char porosity is very close to unity. The CO produced diffuses out of the particle while the decrease in the CO_2 concentration is constantly adjusted by diffusion due to the imposed constant CO_2 pressure at the particle surface. The CO diffuses out of the particle so rapidly that it has no time to accu mulate and cause a pressure increase. In such operating conditions, the gasification reaction characteristic time is far greater than that of reactants/products diffusion [33].

The porosity evolution in the gasification stage is uniform throughout the particle which is synonym of the uniformity of the reaction in the particle. While transfer limitations exists for the pyrolysis stage, the char gasification is performed in a chemically controlled regime.

5.2.3. Model sensitivity

The modelling results can be affected by the meshing size as well as by the model parameters. We first assessed the model sensitivity to the mesh size. Fig. 14 shows the experimental vs. modelling results for three mesh sizes. As depicted on the figure, decreasing the maximum mesh size by 3 folds or doubling it does

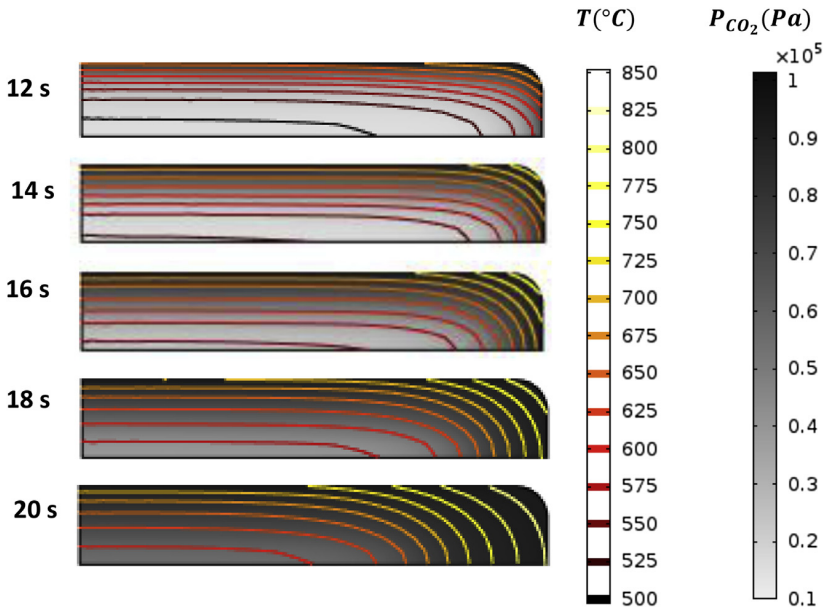

Fig. 13. Colour map plots (Grey scale) of the CO_2 partial pressure in the particle and contour plots (yellow to red contours) of the temperature at 12 s, 14 s, 16 s, 18 s and 20 s. (For interpretation of the references to colour in this figure legend, the reader is referred to the web version of this article.)

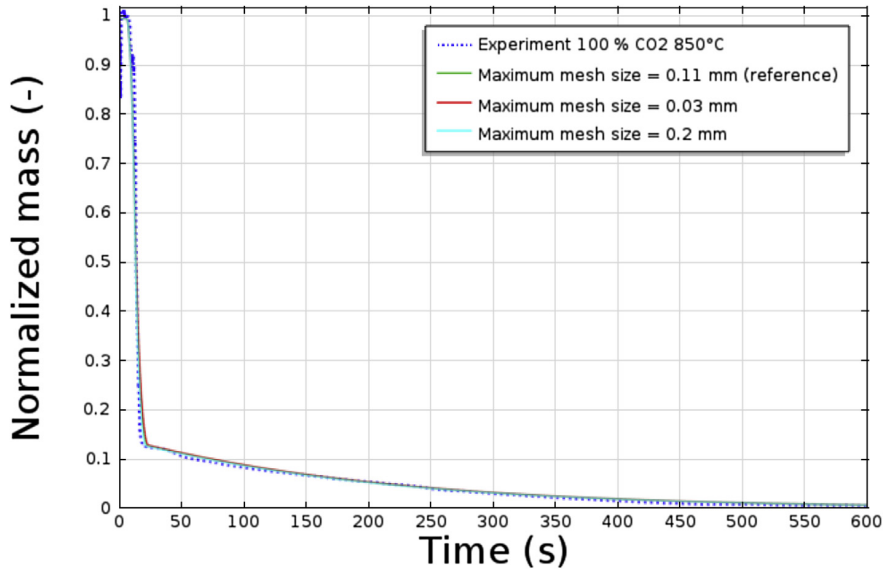

Fig. 14. Influence of the mesh size on the modelling results.

not influence the modelling results.

The sensitivity of normalized mass vs. time results to several model parameters was investigated by modifying them, one at a time. The results are shown in Figs. 15 and 16.

The main results are that the model sensitivity to the $\int(Cp_i \quad Cp_j)dT$ term is quite low. Omitting this term does not modify the modelling result. The model sensitivity to the heat of pyrolysis, convective heat transfer coefficient, wood thermal conductivity as well as particle emissivity is not very marked. However, we found that the model is quite sensitive to the stoichiometric coefficients. The model is not able to capture the end of the pyrolysis reaction when doubling ω_C. Keeping ω_T constant, ω_G varies when ω_C is changed, but with no marked influence on the pyrolysis rate. Increasing k5 impacts on the gasification rate as depicted in Fig. 16.

6. Conclusion

The CO_2 pyro gasification of biomass was studied with the aim to assess the potential of CO_2 valorisation as a gasifying medium in fluidized bed gasifiers. Experimental results obtained for 1 mm thick particles, show that the gasification stage is the rate limiting step in the pyro gasification process. The pyrolysis ended at about 25 s while near to 600 s were necessary to achieve the char gasification reaction. The CO_2 had no major effects on the pyrolysis rate compared to reference pyrolysis in an N_2 atmosphere. After the pyrolysis stage, a 10 s duration plateau was observed before the starting of the char gasification. This plateau was captured by the model. The modelling results show that during this plateau, the CO_2 was present inside the char particle, but the temperature was quite low to induce a starting

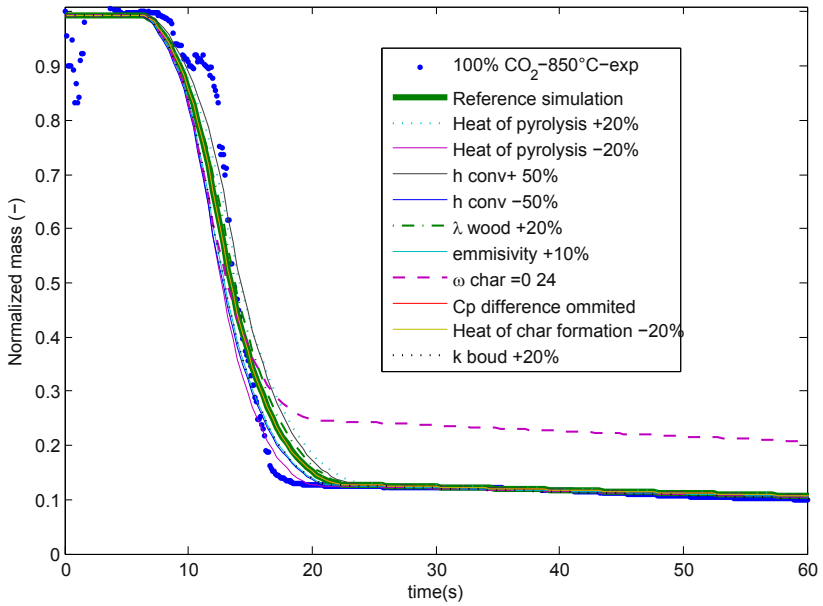

Fig. 15. Sensitivity analysis: focus on the pyrolysis stage.

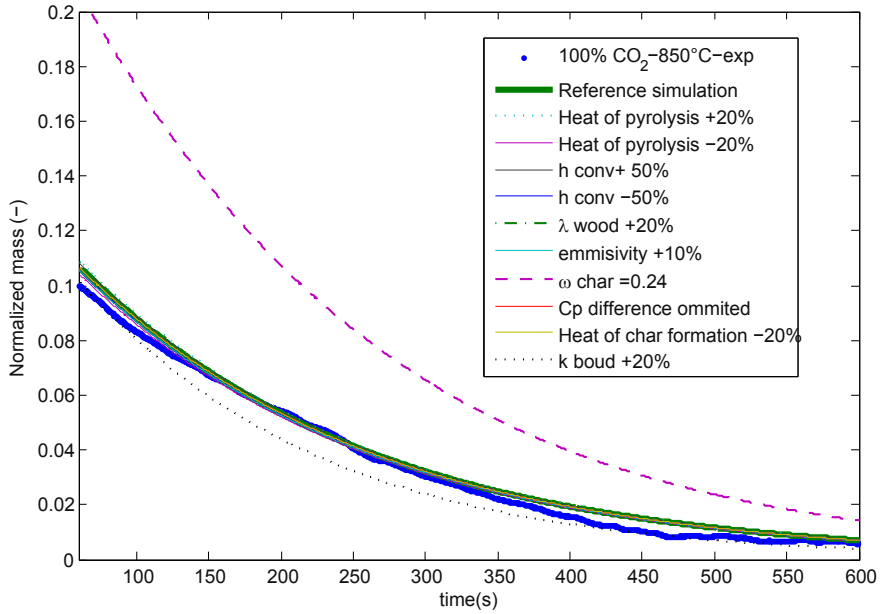

Fig. 16. Sensitivity analysis: focus on the char gasification stage.

of the gasification and a noticeable mass loss. The numerical model developed in this work shed light on the unfolding of the whole pyro gasification of 1 mm thick wood chips. This global approach, for high heating rate conditions, is not tackled in the literature. However, the model still a simplified one. It can be further improved by considering a more extended pyrolysis scheme and considering the interaction of CO_2 with the pyrolysis gas products.

Acknowledgements

The authors acknowledge the National Research Agency ANR (ANR 10 BIOE 0002) France for its financial support in the RECO2 project. They also wish to express their appreciation to Diago Hermano for his help.

Appendix A. Mathematical transformation of the conservation equations

For the "*Transport of diluted species*" COMSOL module, the mass conservation of a gaseous specie "i" is described as:

$$\frac{\partial C_i}{\partial t} + \nabla\cdot(C_i\mathbf{V} \quad D\nabla C_i) \quad R_i \tag{32}$$

In our case, the model variables, there are the densities of the different gaseous species. For the i^{est} gas specie, the conservation

equation reads:

$$\frac{\partial \varepsilon \rho_i}{\partial t} + \nabla \cdot \left(\rho_i \mathbf{v} \quad D_{eff} \nabla \rho_i \right) \quad r_i \tag{33}$$

We define therefore:

$$C_i \quad \varepsilon \frac{\rho_i}{M_i}, \quad \mathbf{V} \quad \frac{\mathbf{v}}{\varepsilon}, \quad D \quad \frac{D_{eff}}{\varepsilon}, \quad R_i \quad r_i / M_i$$

For the "*Heat transfer in fluids*" COMSOL module, the energy conservation equation is written as:

$$\rho C_p \frac{\partial T}{\partial t} + \rho C_p \mathbf{u} \nabla T \qquad \nabla \cdot \mathbf{q} + Q \tag{34}$$

In the present case, the energy conservation equation reads:

$$\left(\rho_B C_{pB} + \rho_C C_{pC} + \varepsilon \rho_G C_{pG} + \varepsilon \rho_T C_{pT} + \varepsilon \rho_{CO_2} C_{pCO_2} \right) \frac{\partial T}{\partial t} + \nabla \cdot \sum_i h_i \mathbf{N}_i$$

$$\nabla \cdot \mathbf{q} + Q$$

Heat transported by the gas species entering and exiting from a volume dV is expressed by:

$$\nabla \cdot \sum_i (h_i \, \mathbf{N}_i) \quad \sum_i \nabla \cdot (h_i \, \mathbf{N}_i)$$

For the i^{est} gas specie, we have:

$$\nabla \cdot (h_i \, \mathbf{N}_i) \quad h_i \nabla \cdot \mathbf{N}_i + \nabla h_i \cdot \mathbf{N}_i \quad \text{and} \quad \nabla h_i \quad Cp_i \, \nabla T + T \, \nabla Cp_i$$

As the specific heat is only temperature dependent, it gives:

$$\nabla Cp_i \quad \mathbf{0}$$

Therefore:

$$\nabla \cdot \sum_i (h_i \, \mathbf{N}_i) \quad \sum_i (Cp_i \, \mathbf{N}_i \, \nabla T) + T \sum_i (Cp_i \, \nabla \cdot \mathbf{N}_i)$$

We define here "A" as:

$$A \quad \sum_i (Cp_i \, \nabla \cdot \mathbf{N}_i)$$

The energy conservation equation becomes:

$$\left(\rho_B C_{pB} + \rho_C C_{pC} + \varepsilon \rho_G C_{pG} + \varepsilon \rho_T C_{pT} + \varepsilon \rho_{CO_2} C_{pCO_2} + \varepsilon \rho_{CO} C_{pCO} \right) \frac{\partial T}{\partial t}$$

$$+ T \, A + \sum_i (Cp_i \, \mathbf{N}_i) \cdot \nabla T \qquad \nabla \cdot \mathbf{q} + Q$$

By identification with the COMSOL formulation we can set:
An equivalent ρCp.

$$(\rho Cp)_{eq} \quad \left(\rho_B C_{pB} + \rho_C C_{pC} + \varepsilon \rho_G C_{pG} + \varepsilon \rho_T C_{pT} + \varepsilon \rho_{CO_2} C_{pCO_2} \right.$$

$$\left. + \varepsilon \rho_{CO} C_{pCO} \right)$$

An equivalent velocity $\mathbf{u}$:

$$\mathbf{u}_{eq} \quad \frac{\sum_i (Cp_i \mathbf{N}_i)}{(\rho Cp)_{eq}}$$

and finally an equivalent heat source term $\tilde{Q}_{eq}$:

$$Q_{iden} \quad Q \quad TA$$

References

[1] R.S. Dhillon, G.V. Wuehlisch, Mitigation of global warming through renewable biomass, Biomass Bioenergy 48 (2012) 75 89.
[2] G. a. Florides, P. Christodoulides, Global Warming and Carbon Dioxide through Sciences, Feb. 2009.
[3] B. Hu, C. Guild, S.L. Suib, Thermal, electrochemical, and photochemical conversion of CO_2 to fuels and value-added products, J. CO_2 Util. 1 (June 2013) 18 27.
[4] P. Basu, Biomass Gasification and Pyrolysis: Practical Design and Theory, Elsevier, 2010.
[5] H.C. Butterman, M.J. Castaldi, Influence of CO_2 injection on biomass gasification, Society (2007) 8875 8886.
[6] H.C. Butterman, M.J. Castaldi, NAWTEC16-1949 CO_2 enhanced steam gasification of biomass fuels, Scanning Electron Microsc. (May 2008) 1 16.
[7] C. Di Blasi, Combustion and gasification rates of lignocellulosic chars, Prog. Energy Combust. Sci. 35 (Apr. 2009) 121 140.
[8] K. Jamil, J.-i. Hayashi, C.-Z. Li, Pyrolysis of a Victorian brown coal and gasification of nascent char in CO_2 atmosphere in a wire-mesh reactor, Fuel 83 (May 2004) 833 843.
[9] B. Prabowo, K. Umeki, M. Yan, M.R. Nakamura, M.J. Castaldi, K. Yoshikawa, CO_2 steam mixture for direct and indirect gasification of rice straw in a downdraft gasifier: laboratory-scale experiments and performance prediction, Appl. Energy 113 (Jan. 2014) 670 679.
[10] H.C. Butterman, M.J. Castaldi, CO_2 as a carbon neutral fuel source via enhanced biomass gasification, Environ. Sci. Technol. 43 (Dec. 2009) 9030 9037.
[11] D. Roberts, D. Harris, Char gasification in mixtures of CO_2 and H_2O: competition and inhibition, Fuel 86 (Dec. 2007) 2672 2678.
[12] Nilsson Susanna, Gómez-Barea Alberto, Diego Fuentes Cano, Gasification reactivity of char from dried sewage sludge in a fluidized bed, Fuel 92 (1) (February 2012) 346 353. ISSN 0016-2361, http://dx.doi.org/10.1016/j.fuel.2011.07.031.
[13] C. Guizani, F. Escudero Sanz, S. Salvador, The gasification reactivity of high-heating-rate chars in single and mixed atmospheres of H_2O and CO_2, Fuel 108 (June 2013) 812 823.
[14] T. Renganathan, M. Yadav, S. Pushpavanam, R. Voolapalli, Y. Cho, CO_2 utilization for gasification of carbonaceous feedstocks: a thermodynamic analysis, Chem. Eng. Sci. 83 (Dec. 2012) 159 170.
[15] M. Pohoelý, M. Jeremiáš, K. Svoboda, P. Kameníková, S. Skoblia, Z. Beo, CO_2 as moderator for biomass gasification, Fuel 117 (Jan. 2014) 198 205.
[16] I. Sircar, A. Sane, W. Wang, J.P. Gore, Experimental and modeling study of pinewood char gasification with CO_2, Fuel 119 (Mar. 2014) 38 46.
[17] P. Ollero, A. Serrera, R. Arjona, S. Alcantarilla, The CO_2 gasification kinetics of olive residue, Biomass Bioenergy 24 (Feb. 2003) 151 161.
[18] A. Gómez-Barea, P. Ollero, C. Fernández-Baco, Diffusional effects in CO_2 gasification experiments with single biomass char particles. 1. Experimental investigation, Energy Fuels 20 (Sept. 2006) 2202 2210.
[19] A.G. Borrego, L. Garavaglia, W. Kalkreuth, Characteristics of high heating rate biomass chars prepared under N_2 and CO_2 atmospheres, Int. J. Coal Geol. 77 (Jan. 2009) 409 415.
[20] H. Zhang, R. Xiao, D. Wang, G. He, S. Shao, J. Zhang, Z. Zhong, Biomass fast pyrolysis in a fluidized bed reactor under N_2, CO_2, CO, CH_4 and H_2 atmospheres, Bioresour. Technol. 102 (Mar. 2011) 4258 4264.
[21] Watanabe Hirotatsu, Shimomura Kiyomi, Okazaki Ken, Effect of high CO_2 concentration on char formation through mineral reaction during biomass pyrolysis, Proc. Combust. Inst. 34 (2) (2013) 2339 2345.
[22] C. Guizani, F.J. Escudero, Sanz S. Salvador, Effects of CO_2 on biomass fast pyrolysis: reaction rate, gas yields and char reactive properties, Fuel 116 (15 January 2014) 310 320.
[23] C. Di Blasi, Modeling chemical and physical processes of wood and biomass pyrolysis, Prog. Energy Combust. Sci. 34 (Feb. 2008) 47 90.
[24] C. Branca, C. Di Blasi, Kinetics of the isothermal degradation of wood in the temperature range 528708 K, J. Anal. Appl. Pyrol. 67 (May 2003) 207 219.
[25] Y. Haseli, J. van Oijen, L. de Goey, Modeling biomass particle pyrolysis with temperature-dependent heat of reactions, J. Anal. Appl. Pyrol. 90 (Mar. 2011) 140 154.
[26] T. Mani, N. Mahinpey, P. Murugan, Reaction kinetics and mass transfer studies of biomass char gasification with CO_2, Chem. Eng. Sci. 66 (Jan. 2011) 36 41.
[27] D.K. Seo, S.K. Lee, M.W. Kang, J. Hwang, T.-U. Yu, Gasification reactivity of biomass chars with CO_2, Biomass Bioenergy 34 (Dec. 2010) 1946 1953.
[28] C. Couhert, J.-M. Commandré, S. Salvador, Failure of the component additivity rule to predict gas yields of biomass in flash pyrolysis at 950C, Biomass Bioenergy 33 (Feb. 2009) 316 326.
[29] A. Sharma, V. Pareek, S. Wang, Z. Zhang, H. Yang, D. Zhang, A phenomenological model of the mechanisms of lignocellulosic biomass pyrolysis processes, Comput. Chem. Eng. 60 (Jan. 2014) 231 241.
[30] G. Gauthier, T. Melkior, M. Grateau, S. Thiery, S. Salvador, Pyrolysis of centimetre-scale wood particles: new experimental developments and results, J. Anal. Appl. Pyrol. 104 (Nov. 2013) 521 530.
[31] H. Bennadji, K. Smith, S. Shabangu, E.M. Fisher, Low-temperature pyrolysis of woody biomass in the thermally thick regime, Energy Fuels 27 (Mar. 2013) 1453 1459.

[32] P. Mousques, J. Dirion, D. Grouset, Modeling of solid particles pyrolysis, J. Anal. Appl. Pyrol. 58 59 (Apr. 2001) 733 745.
[33] S. Septien Stringel, High Temperature Gasification of Millimetric Wood Particles between 800 C and 1400 C, Ph.d. thesis, Université de Toulouse, Institut National Polytechnique de Toulouse, 2011.
[34] F. Mermoud, F. Golfier, S. Salvador, L. Vandesteene, J. Dirion, Experimental and numerical study of steam gasification of a single charcoal particle, Combust. Flame 145 (Apr. 2006) 59 79.
[35] L. Van de steene, J. Tagutchou, F. Mermoud, E. Martin, S. Salvador, A new experimental Continuous Fixed Bed Reactor to characterise wood char gasification, Fuel 89 (Nov. 2010) 3320 3329.
[36] W. Chan, Modeling and experimental verification of physical and chemical process during pyrolysis of a large biomass particle, Fuel 64 (1985) 1505 1513.